Korean J. Chem. Eng., 37(4), 716-723 (2020)
DOI: 10.1007/s11814-019-0352-5

pISSN: 0256-1115
eISSN: 1975-7220

Size control of azilsartan by drowning-out crystallization with phase transformation

Chun-Il Park, Wang-Soo Kim, and Kee-Kahb Koo†

Department of Chemical and Biomolecular Engineering, Sogang University, Seoul 04107, Korea
(*Received 28 May 2019 • accepted 5 August 2019*)

Abstract−To complement the insufficient bioavailability of azilsartan, particle size reduction of azilsartan by drowning-out was attempted. By injecting an azilsartan/ethanol solution into the antisolvent of water, two phases of azilsartan, amorphous and crystalline type A, were found along with phase transformation. The crystal size was strongly affected by the operating parameters such as the volume ratio of antisolvent/azilsartan solution, crystallization temperature, and additives. The crystal size decreased upon increasing the antisolvent/azilsartan solution volume ratio and lowering the temperature. Furthermore, addition of carboxylic acids to the antisolvent of water produced nano-meter sized crystals. In particular, 200 nm particles were obtained with acetic acid. An enhancement in the dissolution rate was found for size-reduced azilsartan crystals, especially when the crystals' sizes were in the nanometer range.

Keywords: Azilsartan, Crystal Size Reduction, Dissolution Rate, Drowning-out Crystallization, Phase Transformation

INTRODUCTION

Azilsartan, which has been approved as an angiotensin receptor blocker (ARB), has potent antihypertensive effects and superior control efficiency for 24-hour systolic BP relative to other well-known ARBs, such as olmesartan, valsartan, and candesartan [1]. However, azilsartan is associated with undesirable physicochemical properties, such as a poor aqueous solubility and a high molecular weight, that potentially lead to lower dissolution rate in biological fluids, and hence a short efficacy in patients, particularly when orally delivered [2].

Particle size reduction facilitates an increase in the interfacial area of drug substances for contacting with the dissolution medium, thereby enhancing the rate of dissolution [3,4]. Additionally, it was experimentally discovered that the diffusion layer decreases as the particle size decreases, leading to faster transport of solvation molecules to the bulk solution and, hence, faster dissolution [5]. One of the promising techniques for particle size reduction is drowning-out crystallization (or antisolvent crystallization). Drowning-out crystallization has been found to modify the solid properties of drug substances including the crystal form and particle size distributions, because the method eliminates the use of thermal energy that may degrade the biological activity of drugs [6,7].

Studies to determine the effect of various operating conditions to control the particle size and dissolution properties of produced particles have been successfully conducted on several ARBs. The process of drowning-out of telmisartan from its dimethyl sulfoxide solution by addition of water was studied by Sharma et al. [8]. They determined that the particle size can be reduced up to the nano-ranges by ultrasound assisted drowning-out crystallization after adjusting of operational parameters, including the sonication time and amplitude, drug solution concentration, antisolvent/solvent ratio, solution injection rate, and crystallization temperature. Similarly, Jain et al. optimized the variable operational conditions to obtain candesartan cilexetil nanocrystals by the drowning-out [9]. Some researchers have focused on the production of size-reduced ARB particles with an amorphous state that have a better dissolution property [10,11]. However, there is an uncontrollable tendency to recrystallize to the more stable crystalline forms during storage or even during the drowning-out process, which may lead to lower the dissolution properties by aggregation of the particles [12,13].

In our previous work, acidification of azilsartan disodium salt in an aqueous solution was proposed to produce submicron-sized azilsartan crystals. However, purity control of final products in this method is very sensitive because of two kinds of byproducts: (1) methanol is generated from the preparation of azilsartan disodium salt aqueous solution, and (2) desethyl azilsartan could be formed by dealkylation of ethoxy group at a low pH condition [14]. On the other hand, in the present work, considering that ethanol is mixed well with methanol and also used as a pretreatment agent for removing desethyl impurities [15], drowning-out crystallization, in which ethanol solution of azilsartan is injected into water (antisolvent), was conducted to obtain azilsartan crystals with an enhanced purity. The influence of the experimental parameters, such as the volume ratio of antisolvent/azilsartan solution, the crystallization temperature, and the additives (carboxylic acids), was investigated by monitoring the solid and liquid phases by focused beam reflectance measurement (FBRM) and UV-visible spectroscopy. The azilsartan crystals were characterized by scanning electron microscopy (SEM), Fourier transform infrared spectroscopy (FT-IR), X-ray diffraction (XRD), and in vitro dissolution rate tests.

EXPERIMENTAL SECTION

1. Materials

Raw azilsartan was supplied by Kolon Life Science, Inc. (Seoul, Korea). Deionized water was purified using a distillation apparatus (Younglin, Ultra 370 series, Korea). Ethanol, formic acid, ace-

†To whom correspondence should be addressed.
E-mail: koo@sogang.ac.kr

tic acid, propionic acid, butyric acid, and a standard buffer solution (pH 7) were supplied by Daejung Chemical & Materials (Seoul, Korea).

2. Solubility Measurements

The solubility of azilsartan in the ethanol/water mixture was measured in the temperature range of 15 to 60 °C. An excess amount of azilsartan was added to 50 g of the ethanol/water mixture or 80 ml of neat ethanol in a vial. The azilsartan solution was maintained in a water bath at a controlled temperature, and stirred with a magnetic bar for at least 24 h. The azilsartan solution was stabilized without mixing for 3 h and the supernatant was filtered through a 0.22 μm HPLC disposable filter under isothermal conditions. The sample solution was kept in a petri-dish and dried at 40 °C until the mass of the sample did not change. The solubility of azilsartan was calculated by the weight difference between the residual mass and the initial solution. All solubility experiments were conducted at least in triplicate.

3. Drowning-out Crystallization of Azilsartan

The azilsartan solution was prepared at 60 °C by dissolving raw azilsartan with saturation concentration in ethanol (22.2 g/*l*). A varying amount of antisolvent (distilled water of 100 to 400 ml) was introduced into a crystallizer that was maintained at a constant temperature of 20, 25, 30, 35, or 40 °C. For the experiments to investigate the effect of the additives, carboxylic acids (formic acid, acetic acid, propionic acid, and butyric acid) were introduced with 0.5 wt% into the antisolvent of water. The drowning-out crystallization was performed by injecting the 20 ml azilsartan solution into the antisolvent using a syringe. The solution was agitated at 400 rpm using an over-head stirrer with three blades. After the experiment, the crystals were separated using a membrane filter with a pore size of 100 nm and dried for 24 h at 40 °C using a vacuum oven.

During crystallization, the azilsartan at 20 °C without any additives was subjected to focused beam reflectance measurement (FBRM, Mettler-Toledo, G400, USA), X-ray diffractometer (XRD, Rigaku, MiniFlex, Japan), and field emission scanning electron microscopy (FE-SEM, JSM-7100F, JEOL, Japan) to monitor the solid phase of azilsartan suspension. The FBRM probe was settled to the crystallizer to observe the particle counts change during the process. The generated azilsartan suspension was intermittently sampled and subjected to XRD and FE-SEM image analysis after washing and drying. To investigate the azilsartan concentration in the liquid sample, the UV absorbance was measured using a UV-visible spectrophotometer (Sinco, S-3100, Korea).

4. Characterization of the Recrystallized Azilsartan

The morphology and size of the azilsartan crystals were observed by scanning electron microscopy (SEM, JEOL, JSM-6010LA, Japan). The azilsartan powder was scattered on a stub with double-sided copper adhesive tape. The samples were coated with gold using a sputter coater (Watford, Cressington Sputter Coater 108 Auto, England). The average crystal size and crystal size distribution (CSD) of the sample powder were determined by measuring at least 300 crystals that were arbitrarily selected from the SEM image.

The molecular state of the azilsartan was analyzed by Fourier transform infrared spectroscopy (FT-IR, Bio Rad, FTS 3000MX, USA) using the traditional transmission technique with KBr pellets. The KBr pellets of the azilsartan samples were prepared in 7 mm diameters by diluting and grinding azilsartan powder (1 mg) with 100 mg of KBr (spectroscopic grade). FT-IR spectra were recorded at a spectral resolution of 4 cm^{-1} with 32 scans for each sample, and the collected spectra were ratioed against air. The average spectrum of each powder sample was used for evaluation.

The crystal structure of azilsartan was investigated to detect any changes in the physical characteristics and the crystallinity of the azilsartan powder was determined using X-ray diffractometer (XRD, Rigaku, MiniFlex, Japan). The sample powder was placed in a glass sample holder and diffraction data were recorded over the 2θ range from 5 to 50° with a step size of 0.02 and a scanning rate of 1.0°/min.

In vitro dissolution tests of the azilsartan crystal samples were performed using the paddle method (USP apparatus type II) with equivalent amounts of azilsartan (5 g) in 900 ml of dissolution medium (pH 7 standard buffer solution). The temperature (37 °C) and paddle-rotation speed (50 rpm) were set accordingly for the dissolution experiments. Samples (5 ml) were withdrawn at time interval of 5, 10, 15, 20, 30, 45, 60, and 90 min using a 0.22 μm HPLC disposable filter and replaced with an equal volume of fresh dissolution medium that was equilibrated at 37°C. The sample concentration was further analyzed by UV detection at a wavelength of 249 nm.

RESULTS AND DISCUSSION

1. Solubility of Azilsartan with Enthalpy-entropy Nonlinear Compensation

The solubility (X, molar concentration) of azilsartan (type A) in the ethanol/water mixture in the temperature range of 15 to 60 °C is shown in Fig. 1. The solubility of azilsartan increased as the temperature and ethanol fraction increased and had a maximum value at an ethanol fraction of approximately 0.9 for all temperatures. The enthalpy-entropy nonlinear compensation can be used to rationalize the mechanism of the molecular interaction and subsequently understand the effect of the mixed composition on the solubility [16,17].

When a van't Hoff plot from the solubility data is fitted well by

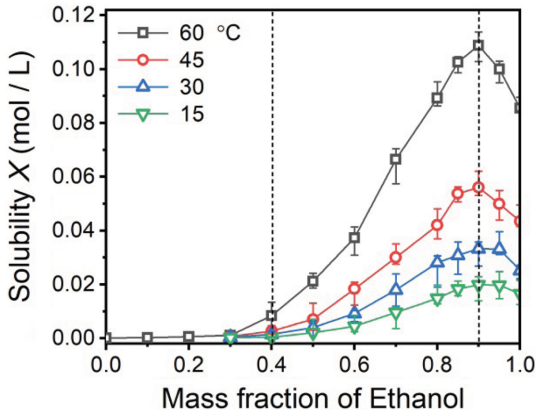

Fig. 1. Solubility (X, molar concentration) of azilsartan in the ethanol/water mixture.

a linear regression, the standard molar enthalpy ($\Delta_{soln}H^o$) and the standard molar free energy ($\Delta_{soln}G^o$) of solution can be derived from each slope and intercept of the van't Hoff plot (regression of ln X against ($1/T-1/T_{hm}$)), according to the Krug approach [18]. The standard molar entropic change for solution ($\Delta_{soln}S^o$) is obtained from the respective $\Delta_{soln}H^o$ and $\Delta_{soln}G^o$ values.

$$\Delta_{soln}H^o = -R \times \text{slope} \quad (1)$$

$$\Delta_{soln}G^o = -RT_{hm} \times \text{intercept} \quad (2)$$

$$\Delta_{soln}S^o = \frac{\Delta_{soln}H^o - \Delta_{soln}G^o}{T_{hm}} \quad (3)$$

where R is the gas constant (8.314 J/mol·K) and T_{hm} is the harmonic mean of the experimental temperature (309.74 K). From the azilsartan solubility data, the van't Hoff plot generally fitted well by the linear model in all cases, which indicates that the van't Hoff equation is reasonable for estimation of the thermodynamic parameters for a solution process ($\Delta_{soln}H^o$, $\Delta_{soln}G^o$, and $\Delta_{soln}S^o$ summarized in Table 1) at T_{hm}. From the estimated values of the thermodynamic parameters, it can be concluded that dissolution of azilsartan in the ethanol/water mixture is endothermic because of the positive $\Delta_{soln}H^o$ in all cases. $\Delta_{soln}S^o$ has positive value except for the mixture from neat water to the 0.2 ethanol fraction, indicating that the overall solution process is entropy driven except with small amounts of ethanol.

The changes in $\Delta_{soln}H^o$ and $\Delta_{soln}G^o$ as a function of the mixture composition are depicted in Fig. 2(a). The plot of $\Delta_{soln}H^o$ is shown to have a different tendency with a sharp increase in the water-rich region (0.0 to 0.4 ethanol fraction), and a smooth decrease in the ethanol-rich region (0.4 to 1.0 ethanol fraction). In contrast $\Delta_{soln}G^o$ consistently decreases. In the water-rich region, the solubility increases although $\Delta_{soln}H^o$ also increases. This phenomenon is the characteristic trend related to hydrophobic solvation with structuring of water molecules around the nonpolar parts of hydrophobic solutes. This water structuring may lower the net heat of mixing, which leads to a small $\Delta_{soln}H^o$, and a large negative $\Delta_{soln}S^o$ owing to the increased order of the surrounding water molecules [19-21]. In the water-rich region, the addition of ethanol to the solution breaks the water structuring, which increases both the enthalpy and entropy. Although the dissolution of solute molecules can be hindered because of the enthalpy increase, a greater increase in entropy counteracts the unfavorable enthalpy change, leading to a slight increase in solubility (entropy driven).

Table 1. Thermodynamic parameters for solution process of azilsartan in the ethanol/water mixtures

Ethanol mass fraction	$\Delta_{soln}H°$ (kJ/mol)	$\Delta_{soln}G°$ (kJ/mol)	$\Delta_{soln}S°$ (kJ/mol)
0.1	5.78	22.32	−53.38
0.2	12.64	20.58	−25.64
0.3	23.64	19.38	13.74
0.4	55.73	16.15	127.77
0.5	40.23	13.22	87.2
0.6	37.51	11.19	84.97
0.7	33.51	9.58	77.24
0.8	30.73	8.61	71.43
0.85	30.33	8.16	71.56
0.9	29.78	7.99	70.32
0.95	27.92	8.13	63.89
1	28.97	8.61	65.73

However, the solubility increase in the ethanol-rich region is driven by the enthalpy decrease, suggesting that the molecular interaction of azilsartan with ethanol predominates. The polarity difference between water and ethanol is one reason for the enhancement in solubility. During the solvation process, the energy of cavity formation is required to break the solvent-solvent interaction. As the ethanol concentration increases, the energy of cavity formation is lowered because the polarity of the solvent mixture is decreased, contributing favorably to the solute-solvent interaction [19]. However, the thermodynamic explanation for the highest solubility for an ethanol fraction of 0.9 is still not clear.

The weighted graph of $\Delta_{soln}H^o$ as a function of $\Delta_{soln}G^o$ is shown in Fig. 2(b). The slope is changed from negative for the water-rich region to positive for the ethanol-rich region (right and left branches based on a 0.4 ethanol fraction). The change in the slope suggests that the variation of solubility is controlled by two different mech-

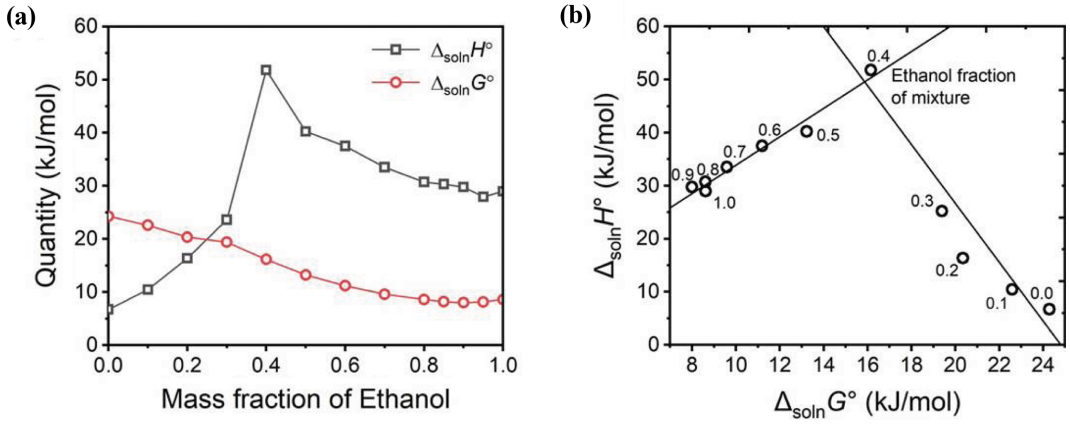

Fig. 2. (a) The standard molar enthalpy ($\Delta_{soln}H^o$) and free energy ($\Delta_{soln}G^o$) of the ethanol/water mixtures, (b) Nonlinear compensation effect for azilsartan in the ethanol/water mixture.

anisms as mentioned above: enthalpy driven (positive slope for the water-rich region) and entropy driven (negative slope for the ethanol-rich region) [19,22].

2. Phase Transformation during Crystallization of Azilsartan

Drowning-out by injection of a drug solution into an antisolvent is widely used in the pharmaceutical industry for particle size reduction because this method induces a higher supersaturation ratio than the reverse injection mode. However, this type of mixing method can possibly generate an unstable amorphous phase [23-25]. In this work, the phase transformation process of azilsartan was also observed with the injection of azilsartan solution (20 ml) into the antisolvent of water (300 ml) at 20 °C. The transition in the solid phase during drowning-out was characterized by analyzing the change in FBRM particle counts, FE-SEM images, and XRD patterns.

As soon as the one-pot injection of azilsartan solution into water, the azilsartan suspension initially appeared as a milky suspension, and small increase in particle counts was observed (Fig. 3(a)). As shown in Fig. 3(c), spherical particles of azilsartan with size of approximately 200 nm were confirmed to be of the amorphous phase (Fig. 3(b)). A small peak in the FBRM counts appeared during the initial 18 min, suggesting that the generated small bubbles and/or agglomerated particles were counted because most of the azilsartan amorphous particles were not large enough for detection. When the FBRM particle counts increased from 18 to 38 min, the spherical amorphous solids gradually changed to larger rod-shaped particles and the XRD pattern of the azilsartan solids showed the characteristic peaks of crystalline type A. This indicates that the transformation process (dissolution of amorphous phase and nucleation with growth of crystalline type A) preceded during this period. No additional changes were observed in the XRD pattern, and the sizes/morphologies of the crystals were observed after 38 min when the particle counts reached equilibrium. Based on these results, the start of transformation, induction time (18 min), and the total transformation time (38 min) were estimated.

Additionally, the azilsartan concentration in the liquid phase was analyzed using the UV-vis spectrophotometer (Fig. 3(a)). After injection of the azilsartan/ethanol solution, the azilsartan concentration rapidly decreased to the equilibrium concentration of the amorphous phase and maintained constantly. The azilsartan concentration began to decrease at 25 min and reached the equilibrium concentration of crystalline type A at 40-45 min. Considering the change in both the solid and liquid phases, the equilibrium state of the azilsartan amorphous phase may have instantly developed and afterwards transformation, indicating nucleation of the crystalline phase is a rate-limiting factor in the drowning-out process. Because the decrease in the azilsartan concentration in the liquid was detected later than the observation of azilsartan crystals in the solid phase, it is expected that nucleation and growth of crystals govern the phase transformation process during crystallization and the dissolution rate is fast enough to prevent the decreasing azilsartan concentration from consumption by the generation of azilsartan crystals [26].

3. Effect of Operating Conditions on the Azilsartan Crystal Size

3-1. Volume Ratio of Antisolvent to the Azilsartan Solution

SEM images of the azilsartan crystals and their cumulative size distribution with the volume ratio of antisolvent to azilsartan solution are shown in Fig. 4. The sizes of the azilsartan crystals notably decreased from about 30 to 5 μm with increasing the antisolvent/azilsartan solution volume ratio from 5 to 15. However, a further increase in this ratio did not result in much difference in crystal size or size distribution.

The volume ratio of antisolvent to drug solution is an important parameter during drowning-out that can affect both the supersaturation ratio (S) and diffusion distance of molecules to growing crystal surface. The supersaturation ratio (S) can be calculated via

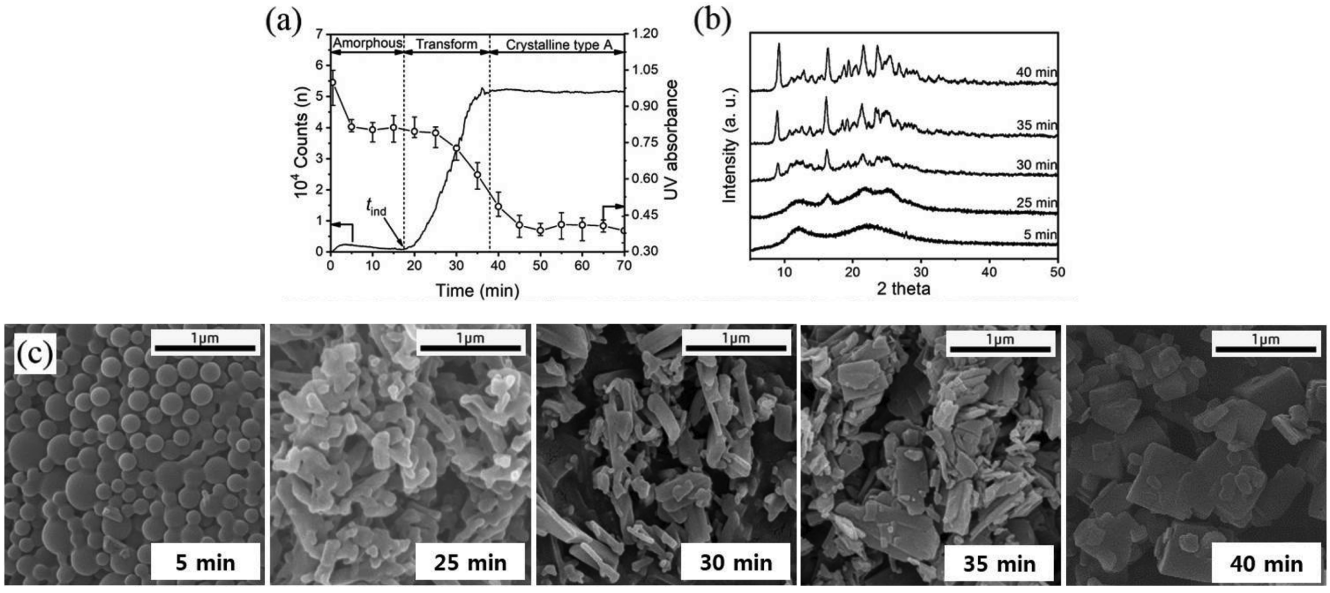

Fig. 3. Monitoring of drowning-out crystallization of azilsartan: (a) Particle counts (solid line) and azilsartan concentration (open circle), (b) XRD patterns and (c) FE-SEM images of the azilsartan particles.

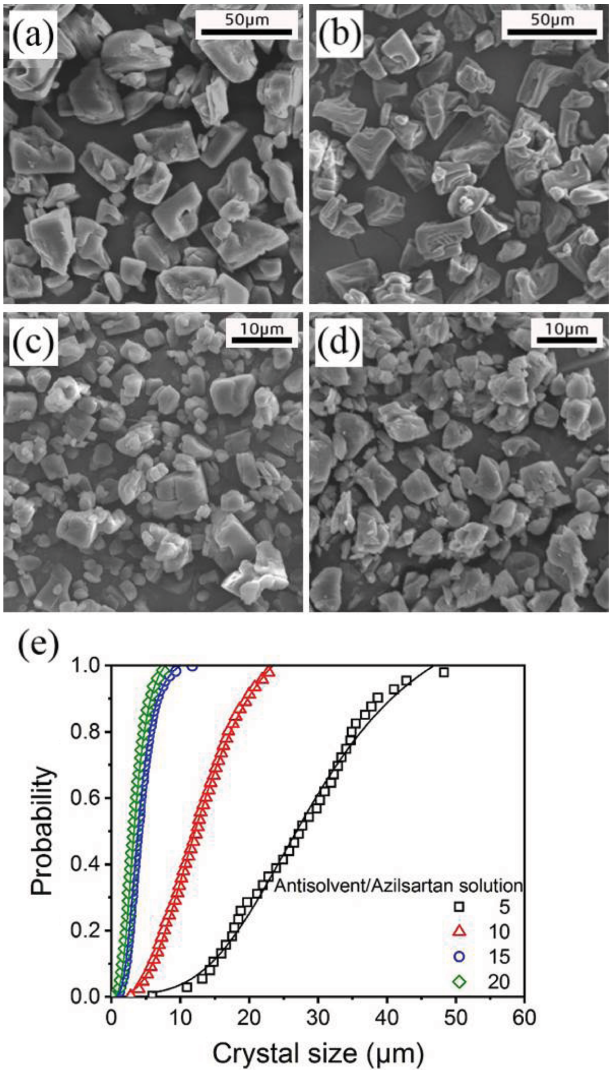

Fig. 4. SEM images of azilsartan crystals for volume ratios of the antisolvent/azilsartan solution of (a) 5, (b) 10, (c) 15, (d) 20, and (e) their cumulative size distributions.

the following equation:

$$S = \frac{C}{C^*} \quad (4)$$

where C and C^* are the azilsartan concentration in ethanol and the saturation concentration of azilsartan in the ethanol/water mixture, respectively. The crystallization process involves two dominant steps: nucleation and crystal growth. Because both nucleation and crystal growth kinetics share the generated supersaturation, the growth rate tends to be small when nucleation vigorously occurs [27]. When a high level of supersaturation is developed at the initial stage of crystallization, the supersaturation is more consumed at nucleation rather than crystal growth, which leads to the production of a large amount of critical nuclei.

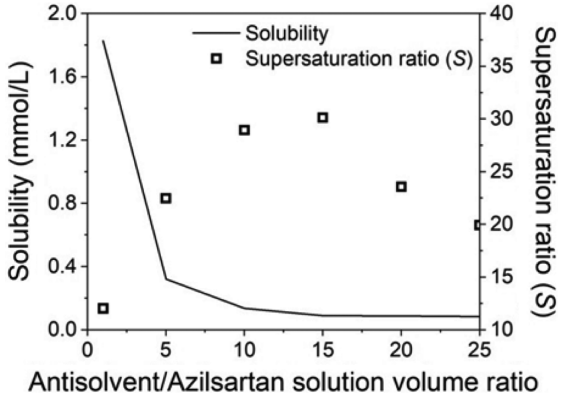

Fig. 5. Effect of the antisolvent/azilsartan solution volume ratio on the terminal solubility of azilsartan in the ethanol/water mixture and the terminal value of the supersaturation ratio (S).

The effect of the antisolvent/azilsartan solution volume ratio on the supersaturation ratio (S) is shown in Fig. 5. As the antisolvent/azilsartan solution volume ratio increased up to 15, the supersaturation ratio (S) increased due to the drastic decrease in solubility in ethanol/water mixture. However, a further increase in the antisolvent amount led to a decrease in the azilsartan concentration in the terminal ethanol/water mixture, while the solubility of the ethanol/water mixture similarly remained consistent, leading to a decrease in the supersaturation level. On the other hand, the increased volume ratio of antisolvent decreased the azilsartan concentration in the ethanol/water mixture and increased the diffusion distance of azilsartan molecules to the surface of the azilsartan crystals. Thus molecular diffusion became the limiting step for the growth of the nuclei [28]. Even though the supersaturation ratio (S) decreased from the antisolvent volume ratio of 15, the increased molecular diffusion distance counteracted the effect of the decreased supersaturation, resulting in smaller azilsartan crystals. However, the crystal sizes were similar for the antisolvent/azilsartan solution volume ratios of 15 and 20; thus, the optimum condition was deter-

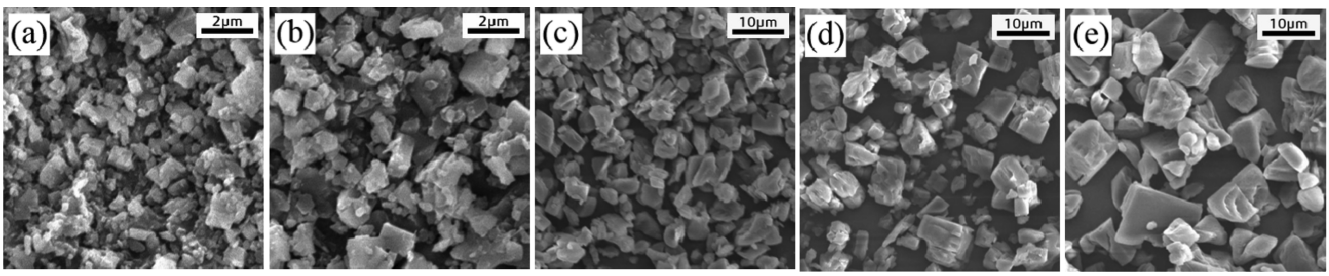

Fig. 6. SEM images of the azilsartan crystals with temperature: (a) 20, (b) 25, (c) 30, (d) 35, and (e) 40 °C.

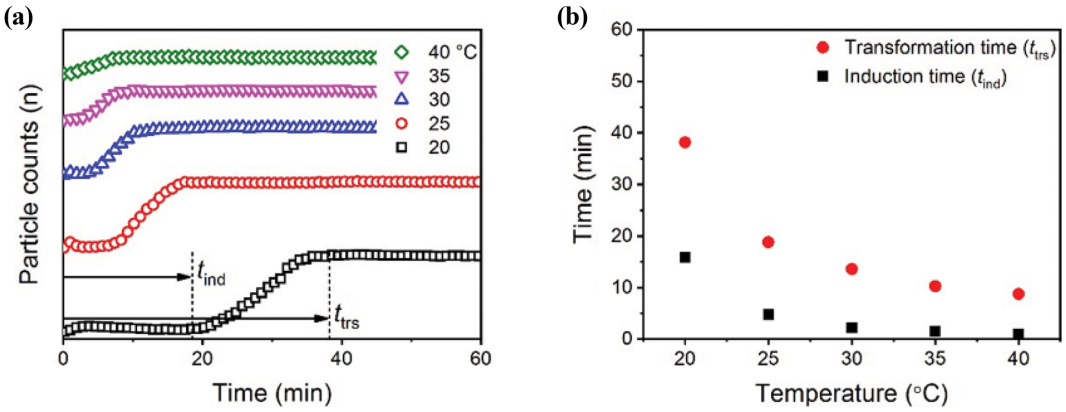

Fig. 7. Phase transformation of azilsartan as a function of temperature: (a) Particle counts measured by FBRM during crystallization, (b) induction and transformation time (t_{ind}, t_{trs}).

mined to be a volume ratio of 15.

3-2. Crystallization Temperature

The mean crystal size of azilsartan decreased from 6.31 to 0.87 μm as the temperature of the ethanol/water mixture decreased from 40 to 20 °C as shown in Fig. 6. As the temperature of the ethanol/water mixture decreased, the solubility of azilsartan decreased, which resulted in higher supersaturation. Simultaneously, the diffusion and growth at the crystal surface may have been retarded due to the decrease in molecular mobility. Therefore, a decrease in the temperature led to small crystal sizes with a narrow size distribution [28].

However, the decrease in temperature caused a delay in the overall phase transformation process (Fig. 7). The phase transformation is initially driven by the thermodynamic driving force (ΔG). The thermodynamic driving force (ΔG) for transformation is defined as the free energy difference between the amorphous phase and crystalline type A, which can be written as follows [26,29]:

$$\Delta G = RT\ln\frac{f_{crys}}{f_{amor}} = RT\ln\frac{a_{crys}}{a_{amor}} \approx RT\ln\frac{x_{crys}}{x_{amor}} \quad (5)$$

where subscripts 'amor' and 'crys' represent amorphous and crystalline type A, respectively, f is the fugacity, a is the thermodynamic activity, x is the saturation concentration of each phase, R is the gas constant (8.314 J/mol·K), and T is the temperature (K).

The values of the thermodynamic driving force (ΔG) and induction time (t_{ind}) for transformation are listed in Table 2. As the temperature increased, both the induction time (t_{ind}) and the absolute value of the thermodynamic driving force (ΔG) for transformation decreased, which is counterintuitive. Phase transformation can be affected by not only the driving force but also other properties, such as molecular mobility. In general, molecular mobility is known to be accelerated by a higher temperature, which can facilitate the phase transformation process [26,29,30].

Table 2. Thermodynamic driving force (ΔG) and induction time (t_{ind}) for the transformation over the temperature range of 20-40 °C

T (°C)	x_{amor} (g/l)	x_{crys} (g/l)	$\Delta G = RT\ln\frac{x_{crs}}{x_{amor}}$ (kj/mol)	t_{ind} (s)
20	0.0601	0.0166	−3.19	950
25	0.0633	0.0201	−2.89	285
30	0.0655	0.0256	−2.41	130
35	0.0674	0.0331	−1.85	95
40	0.0687	0.0363	−1.67	60

Based on classical nucleation theory, the heterogeneous nucleation rate of azilsartan can be expressed as:

$$J = N_0\, V \exp\left(-\frac{\Delta G_{crit}\varphi}{kT}\right) \quad (6)$$

where J is the number of nuclei formed per unit time per unit volume, N_0 is the number of solute molecules per unit volume, ΔG_{crit} is the free energy barrier for formation of the critical nucleus, φ is the heterogeneous nucleation factor, k is the Boltzmann constant (1.3805×10^{-23} J/K), and T is the temperature (K). The frequency of molecular transport at the nucleus-liquid interface, V, can be related to the bulk viscosity, η, via the Stokes-Einstein relation [31].

$$V \approx \frac{kT}{3\pi a_o^3 \eta(T)} \quad (7)$$

where a_o is the mean effective diameter of the diffusing species. The $N_0 \cdot V$ term is also known as the collision factor, A, which represents the rate of attachment of molecules to the critical nucleus. The influence of temperature on the collision factor can be quite significant because the temperature controls both the solution concentration and molecular mobility. As the temperature increased, the solute concentration, N_0, increased because the solubility of the amorphous phase of azilsartan increased. Moreover, the frequency of molecular transport at the nucleus-liquid interface, V, increased because of the increased temperature and decreased solution viscosity. Therefore, the collision factor, A, may increase more than enough to compensate for the decreasing driving force as the temperature increases, leading to faster nucleation.

3-3. Effect of the Carboxylic Acid Additives

As shown in Fig. 8, the carboxylic acid additives can drastically reduce the sizes of azilsartan crystals without modifying the pro-

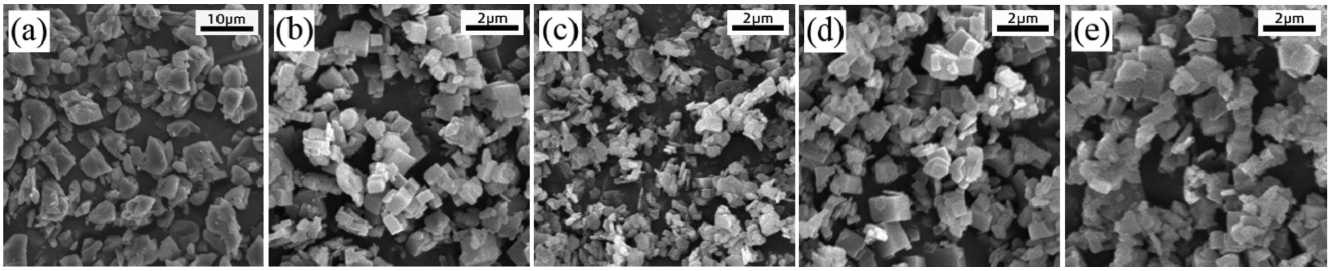

Fig. 8. SEM images of the azilsartan crystals with additives (0.5 wt% of water) at 400 rpm, 30 °C: (a) no additive (b) formic acid, (c) acetic acid, (d) propionic acid, and (e) butyric acid.

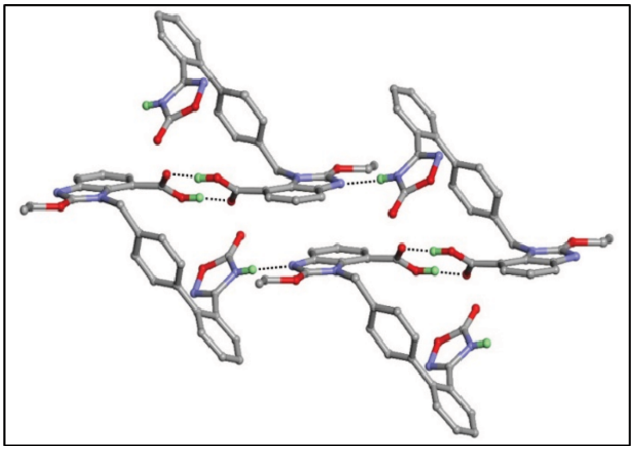

Fig. 9. Tetramer formation of azilsartan molecules in crystalline type A [30].

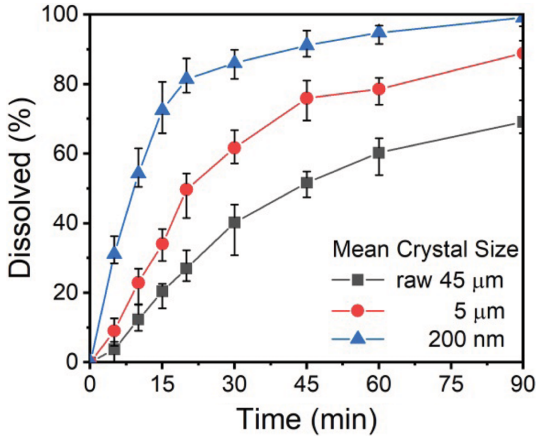

Fig. 10. Dissolution profiles of azilsartan crystals with crystal size.

cess design. The mean sizes of the azilsartan crystals obtained with carboxylic acids were measured to be approximately 200 nm (acetic acid), 400 nm (formic acid), 500 nm (propionic acid) and 700 nm (butyric acid), which are very small compared with the 3.47 μm crystals obtained without additives.

The solubility of azilsartan has been reported to be reduced in acidic conditions, which can be applied to obtain higher supersaturation condition during drowning-out [4]. However, a size reduction of azilsartan crystals with acids such as sulfuric acid, hydrochloric acid, and phosphoric acid was not observed, indicating that the higher supersaturation induced by addition of acids is not the reason for the size reduction effect. We suggest that the azilsartan molecules uniquely interact with carboxylic acids, which can disturb the azilsartan crystal growth. The azilsartan crystal structure is constituted of tetramers via hydrogen bonding of two carboxylic groups (-COOH) and two heterocyclic amines (-NH), which are the main molecular interaction in the azilsartan crystal lattice as shown in Fig. 10 [32]. During crystallization, carboxylic acids with a small molecular size may easily interact with the carboxylic group of azilsartan via hydrogen bonding and hinder the packing of azilsartan molecules, leading to a smaller crystal size.

4. Characterization of Recrystallized Azilsartan

The FT-IR spectrum and XRD pattern of recrystallized azilsartan with acetic acid, which was identical to that of raw azilsartan of crystalline type A [32], suggests that the chemical composition and crystal structure of azilsartan is not affected by the usage of carboxylic acids during drowning-out crystallization (Figs. S1 and S2 in the supporting information). The amorphous intermediates of azilsartan show a low intensity halo (amorphous halo) with no distinct peaks.

It has been widely reported that poorly water-soluble drugs that are a smaller size exhibit a higher dissolution ability, which leads to better bioavailability [6,7]. Fig. 10 shows the *in vitro* dissolution profiles of azilsartan measured using the paddle method. The dissolved amount of azilsartan samples at 30 min is depicted as 86, 61, and 40% with mean crystal sizes of 200 nm, 5 μm, and 45 μm, respectively, showing that the dissolution property is enhanced significantly for crystal size in the nanometer range.

CONCLUSIONS

Azilsartan fine crystals were produced by drowning-out. When an azilsartan/ethanol solution was injected into water, milky solid particles formed immediately, which were amorphous intermediates; they subsequently transformed to type A crystals. In this system, a reduction in the crystal size was observed with an increase in the volume ratio of antisolvent to the azilsartan solution and a decrease in temperature. However, a decrease in temperature led to a slower phase transformation, which increased the overall crystallization time. However, the crystal size of azilsartan can be significantly reduced with carboxylic acids without process delays; in particular, 200 nm sized crystals were produced with addition of acetic acid. There was no change in composition or crystal struc-

ture of the final azilsartan products according to FT-IR and XRD analyses. The dissolution rate of the recrystallized azilsartan crystals was found to improve as the crystal size decreased. Therefore, drowning-out crystallization was shown to be a feasible method to achieve better bioavailability of azilsartan by reducing the crystal size to the nano-meter range.

ACKNOWLEDGEMENT

This work was supported by Kolon Life Science, Inc. (Seoul, Korea).

NOMENCLATURE

Roman Symbols

A : collision factor [$m^{-3}s^{-1}$]
a_o : mean effective diameter [m]
C : concentration of azilsartan in ethanol [mmol L^{-1}]
C^* : saturation concentration of azilsartan in the ethanol/water mixture [mmol L^{-1}]
J : heterogeneous nucleation rate [$m^{-3}s^{-1}$]
k : heterogeneous nucleation rate [J K^{-1}]
N_0 : number of solute molecules per unit volume [m^{-3}]
R : gas constant [$Jmol^{-1}$ K^{-1}]
S : solubility of azilsartan [-]
T : temperature [K]
T_{hm} : harmonic mean of the experimental temperature [K]
t_{ind} : induction time [s]
t_{trs} : total phase transformation time [s]
V : frequency of molecular transport at the nucleus-liquid interface [s^{-1}]
X : solubility of azilsartan [mol L^{-1}]
x : azilsartan saturation concentration of ethanol/water mixture [g L^{-1}]

Greek Symbols

ΔG : thermodynamic driving force for phase transformation [kJ mol^{-1}]
ΔG_{crit} : critical free energy for nucleation [J]
$\Delta_{soln}H^o$: standard molar enthalpy of solution [kJ mol^{-1}]
$\Delta_{soln}G^o$: standard molar free energy of solution [kJ mol^{-1}]
$\Delta_{soln}S^o$: standard molar entropic change of solution [J mol^{-1} K^{-1}]
η : heterogeneous nucleation rate [kg $m^{-1}s^{-1}$]
φ : heterogeneous nucleation factor [-]

SUPPORTING INFORMATION

Additional information as noted in the text. This information is available via the Internet at http://www.springer.com/chemistry/journal/11814.

REFERENCES

1. T. W. Kurtz and T. Kajiya, *Vasc. Health Risk Manage*, **8**, 133 (2012).
2. N. Blagden, M. de Matas, P. T. Gavan and P. York, *Adv. Drug Deliv. Rev.*, **59**(7), 617 (2007).
3. A. A. Noyes and W. R. Whitney, *J. Am. Chem. Soc.*, **19**(12), 930 (1897).
4. T. Lu, Y. Sun, D. Ding, Q. Zhang, R. Fan, Z. He and J. Wang, *AAPS J.*, **18**(2), 473 (2017).
5. A. P. Tinke, K. Vanhoutte, R. De Maesschalck, S. Verheyen and H. De Winter, *J. Pharm. Biomed. Anal.*, **39**(5), 900 (2005).
6. S. Verma, R. Gokhale and D. J. Burgess, *Int. J. Pharm.*, **380**(1-2), 216 (2009).
7. N. Rasenack and B. W. Müller, *Pharm. Dev. Technol.*, **9**(1), 1 (2004).
8. C. Sharma, M. A. Desai and S. R. Patel, *Cryst. Res. Technol.*, **53**(3), 1800001 (2018).
9. S. Jain, V. A. Reddy, S. Arora and K. Patel, *Drug Deliv. Transl. Res.*, **6**(5), 498 (2016).
10. Q. Ma, H. Sun, E. Che, X. Zheng, T. Jiang, C. Sun and S. Wang, *Int. J. Pharm.*, **441**(1-2), 75 (2013).
11. Z. Zhang, Y. Le, J. Wang, H. Zhao and J. Chen, *Particuology*, **10**(4), 462 (2012).
12. B. C. Hancock and G. Zografi, *Pharm. Res.*, **11**, 471 (1994).
13. H. K. Chan and N. Y. Chew, *Adv. Drug Deliv. Rev.*, **55**, 793 (2003).
14. W.-S. Kim and K.-K. Koo, *Cryst. Growth Des.*, **19**, 1797 (2019).
15. A. V. R. Reddy, S. Garaga, C. Takshinamoorthy, G. Gupta and A. Naidu, *Indo Am. J. Pharm. Res.*, **5**(6), 2208 (2015).
16. E. Tomlinson, *Int. J. Pharm.*, **13**, 115 (1983).
17. E. Tomlinson and S. S. Davis, *J. Colloid Interface Sci.*, **76**, 563 (1980).
18. R. R. Krug, W. G. Hunter and R. A. Grieger, *J. Phys. Chem.*, **80**, 2341 (1976).
19. P. Bustamante, S. Romero, A. Peña, B. Escalera and A. Reillo, *J. Pharm. Sci.*, **87**, 1590 (1998).
20. A. C. Rouw and G. Somsen, *J. Solution Chem.*, **10**, 533 (1981).
21. W. J. M. Heuvelsland, C. de Visser and G. Somsen, *J. Phys. Chem.*, **82**, 29 (1978).
22. F. Martíneza, M. Á. Peña and P. Bustamante, *Fluid Phase Equilib.*, **308**, 98 (2011).
23. H. H. Tung, E. L. Paul, M. Midler and J. A. McCauley, *Crystallization of organic compounds: an industrial perspective*, Wiley, NewYork (2009).
24. L. Lindfors, P. Skantze, U. Skantze, M. Rasmusson, A. Zackrisson and U. Olsson, *Langmuir*, **22**(3), 906 (2006).
25. D. Erdemir, A. Y. Lee and A. S. Myerson, *Acc. Chem. Res.*, **42**(5), 621 (2009).
26. A. Maher, D. M. Croker, Å. C. Rasmuson and B. K. Hodnett, *Cryst. Growth Des.*, **12**(12), 6151 (2012).
27. J. W. Kim, J. K. Kim, H. S. Kim and K. K. Koo, *Cryst. Growth Des.*, **9**(6), 2700 (2009).
28. M. Kakran, N. G. Sahoo, I. L. Tan and L. Li, *J. Nanoparticle Res.*, **14**(3), 757 (2012).
29. W. Du, Q. Yin, H. Hao, Y.Bao, X. Zhang, J. Huang, X. Li, G. Xie and J. Gong, *Ind. Eng. Chem. Res.*, **53**(14), 5652 (2014).
30. C. H. Gu and V. Young, *J. Pharm. Sci.*, **90**(11), 1878 (2001).
31. N. Rodríguez-hornedo and D. Murphy, *J. Pharm. Sci.*, **88**(7), 651 (1999).
32. X. R. Zhang and L. Zhang, *J. Mol. Struct.*, **1137**, 320 (2017).